nature astronomy

Article

https://doi.org/10.1038/s41550-022-01866-x

Laser desorption mass spectrometry with an Orbitrap analyser for in situ astrobiology

Received: 3 January 2022

Accepted: 16 November 2022

Published online: 16 January 2023

Check for updates

Ricardo Arevalo Jr[1] ✉, Lori Willhite[1], Anais Bardyn[1], Ziqin Ni[1], Soumya Ray[1], Adrian Southard[2], Ryan Danell[3], Andrej Grubisic[4], Cynthia Gundersen[5], Niko Minasola[5], Anthony Yu[4], Molly Fahey[4], Emanuel Hernandez[4], Christelle Briois[6], Laurent Thirkell[6], Fabrice Colin[6] & Alexander Makarov[7]

Laser desorption mass spectrometry (LDMS) enables in situ characterization of the organic content and chemical composition of planetary materials without requiring extensive sample processing. Coupled with an Orbitrap analyser capable of ultrahigh mass-resolving powers and accuracies, LDMS techniques facilitate the orthogonal detection of a wide range of biomarkers and classification of host mineralogy. Here an Orbitrap LDMS instrument that has been miniaturized for planetary exploration is shown to meet the performance standards of commercial systems and exceed key figures of merit of heritage spaceflight technologies, including those baselined for near-term mission opportunities. Biogenic compounds at area densities relevant to prospective missions to ocean worlds are identified unambiguously by redundant measurements of molecular ions (with and without salt adducts) and diagnostic fragments. The derivation of collision cross-sections serves to corroborate assignments and inform on molecular structure. Access to trace elements down to parts per million by weight levels provide insights into sample mineralogy and provenance. These analytical capabilities position the miniaturized LDMS described here for a wide range of high-priority mission concepts, such as those focused on life detection objectives (for example, Enceladus Orbilander) and progressive exploration of the lunar surface (for example, via the NASA Artemis Program).

Future astrobiology missions to Europa, Enceladus and other potentially viable ocean worlds will be challenged to distinguish biological signatures without bias towards features associated with terrestrial life[1]. Payload instruments need to support agnostic and discovery-based approaches to distinguish relics of biological processes from the limited complexity and apparent randomness of abiotic sources[2]. A critical capability of next-generation technologies will be the orthogonal (or independent) detection of a variety of biomarkers, including (but not limited to): organic abundance patterns, stable isotope ratios, biogenic minerals and morphologies indicative of microbial activity[3]. Multiple distinct proxies observed across a range of spatial scales provide a framework to gauge the probability of biogenicity[4].

Laser desorption mass spectrometry (LDMS) enables investigations into the organic inventory and the elemental/isotopic composition of planetary materials in situ, providing: (1) access to multiple classes of biomarkers, most notably refractory organic matter, and (2) identification of host mineralogy, ergo geological context for detected organic compounds. Unsupervised data-driven approaches

[1]University of Maryland, College Park, MD, USA. [2]CRESST II, College Park, MD, USA. [3]Danell Consulting, Winterville, NC, USA. [4]NASA Goddard Space Flight Center, Greenbelt, MD, USA. [5]AMU Engineering, Miami, FL, USA. [6]Laboratoire de Physique et Chimie de l'Environnement et de l'Espace, Orléans, France. [7]Thermo Fisher Scientific, Bremen, Germany. ✉e-mail: rarevalo@umd.edu;

https://doi.org/10.1038/s41550-022-01866-x

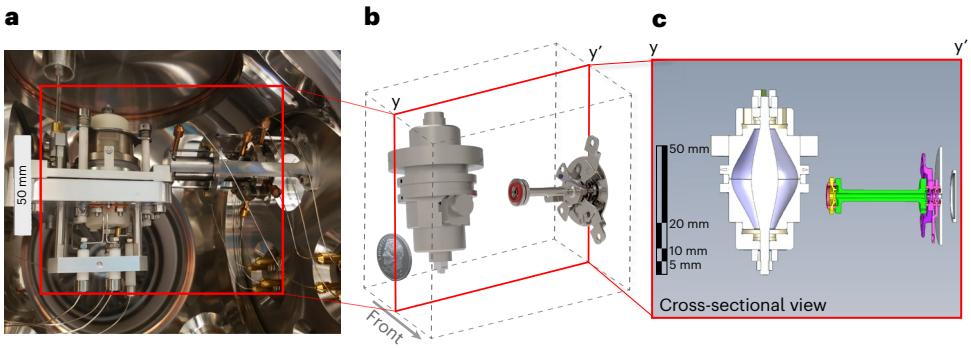

Fig. 1 | The highly miniaturized LDMS instrument described here leverages an Orbitrap mass analyser to achieve ultrahigh mass resolution and accuracy. This prototype, which was designed to minimize mass, volume and power requirements without compromising the capabilities of the proof-of-concept breadboard reported previously[12], exceeds key performance metrics of the MOMA flight instrument[9], including: mass resolution and accuracy, laser output energy and dual-polarity ion detection. **a**, Photograph of the Orbitrap analyser and ion optical lenses mounted within a planetary simulation chamber. **b**,**c**, Solid model (**b**) and cross-sectional view (**c**) showing the orientation and compact geometry of the analyser, lens stack and sample plate.

can increase operational autonomy and enhance confidence in organic/inorganic assignments[5]. Laser microprocessing is well suited for life detection objectives as such methods require minimal sample processing and support two-dimensional chemical imaging without requiring physical contact with the sample; standoff instruments reduce the risk of cross-contamination and planetary protection violations. The spatial resolution of an LDMS experiment is controlled by the profile of the beam focused onto the sample surface, allowing for targeted analyses of micrometre-scale mineral phases, individual dust particles, microfossils, finely laminated biofabrics and discrete strata captured in sample cores. Each laser shot only ablates the uppermost <100 nm of the sample even at elevated fluences[6], resulting in an effective sample mass on the order of nanograms; thus, LDMS is ideal for surface analysis and/or depth profiling. However, this can be a limiting capability if bulk measurements are required to meet specific planetary science objectives.

Due to these analytical advantages, a standoff LDMS instrument called LIMA-D was launched onboard Phobos 2 in 1988; however, communication with the spacecraft was lost during the approach towards Phobos, compromising the mission[7]. A derivative of LIMA-D, named LAZMA[8], was later launched in 2011 onboard the Phobos–Grunt mission, but a propulsion failure left the spacecraft stranded in low Earth orbit. Thus, LDMS techniques have yet to be applied in an extraterrestrial planetary environment. However, LDMS instruments have been developed for the ExoMars rover[9], Dragonfly rotorcraft[10] and Luna-Glob (Luna-25) and Luna-Resurs-1 (Luna-27) missions[11], illustrating the impetus to exploit such in situ techniques to address high-priority science questions in the planetary community.

Here we describe an LDMS instrument that combines an Orbitrap mass analyser, solid-state UV (266 nm) laser system derived from heritage designs, and custom series of ion optics that accelerate and focus ions generated at the sample surface into the analyser (Supplementary Figs. 1–4). A prototype of the LDMS instrument (Fig. 1) has been highly miniaturized relative to the proof-of-concept breadboard reported previously[12] but without a compromise in analytical performance (as discussed further below), representing an engineering model of a spaceflight design that fits within the limited resources expected for a mission to the outer Solar System (for example, the Europa Lander[13]; Supplementary Fig. 5).

The Orbitrap™ analyser, originally developed for commercial laboratories[14] but recently adapted for planetary applications[12], delivers 100× higher mass resolution and mass accuracy compared with the legacy quadrupole sensors that have explored the inner and outer reaches of the Solar System[15]. Such analytical capabilities are essential to separate isobaric interferences (defined by the same nominal mass-to-charge ratio, or integer m/z) and unambiguously identify molecular stoichiometry without additional subsystems (for example, resonance lasers and gas chromatographs). Because the Orbitrap analyser uses electrostatic fields to trap ions[16], the sensor does not require magnets, radio frequency (RF) electronics or consumable detectors, limiting failure modes and minimizing resource requirements. The basic operation of the Orbitrap analyser involves injection and trapping of analyte ions, which then exhibit harmonic axial oscillations at frequencies proportional to $(m/z)^{-½}$. Ion motion recorded as image current in the time domain transient can be converted into frequency space via fast Fourier transform (FFT).

The effective mass range in a given experiment is influenced by the distance the ions travel from the source to the trap and the timing and slew rate of the voltages applied to the centre and deflector electrodes, which together enable electrodynamic squeezing of the incoming ions[14]. During an LDMS analysis, the primary limit to the upper end of the mass range is the capacity of the laser source to ionize macromolecular organic material without incurring excessive fragmentation of the parent molecule. The mass-resolving power is controlled principally by the observation time (that is, transient length) and temporal spread within a single m/z ion packet. Given these timing requirements and sensitivity to temporal smearing, a pulsed laser system is a natural choice to serve as an ion source.

Previously, an Orbitrap analyser extracted from its commercial packaging and interfaced directly to an industrial laser was shown to characterize the mineralogy of a variety of planetary analogue samples and detect amino acids down to <100 fmol mm^{-2} concentrations (based on signal-to-noise ratios (S/Ns)) with only a single laser shot and no spectral stacking[17]. However, this breadboard was not designed to minimize mass, volume and power requirements, but rather to validate experimentally the scientific reach of LDMS techniques that leverage an ultrahigh-resolution mass analyser.

In comparison, the footprint of the LDMS instrument described here has been miniaturized for mission science by interfacing an Orbitrap analyser with a laser system that leverages the side-pumped Cr:Nd:YAG (chromium- and neodymium-doped yttrium aluminum garnet) oscillator design flown on the Lunar Orbiter Laser Altimeter[18], with a fundamental wavelength of 1,064 nm and nominal pulse width of 5 ns. A fourth harmonic generator produces an output wavelength of 266 nm (4.7 eV per photon), enhancing photon–substrate coupling with aromatic organics[19] and many geological phases[20]. The laser generates >450 μJ per pulse at 266 nm (ref. 21), more than three times the maximum energy of the laser for the state-of-the-art Mars Organic Molecule Analyzer (MOMA) instrument onboard the ExoMars rover[9]. Fine attenuation control down to 1% of the maximum output energy is

https://doi.org/10.1038/s41550-022-01866-x

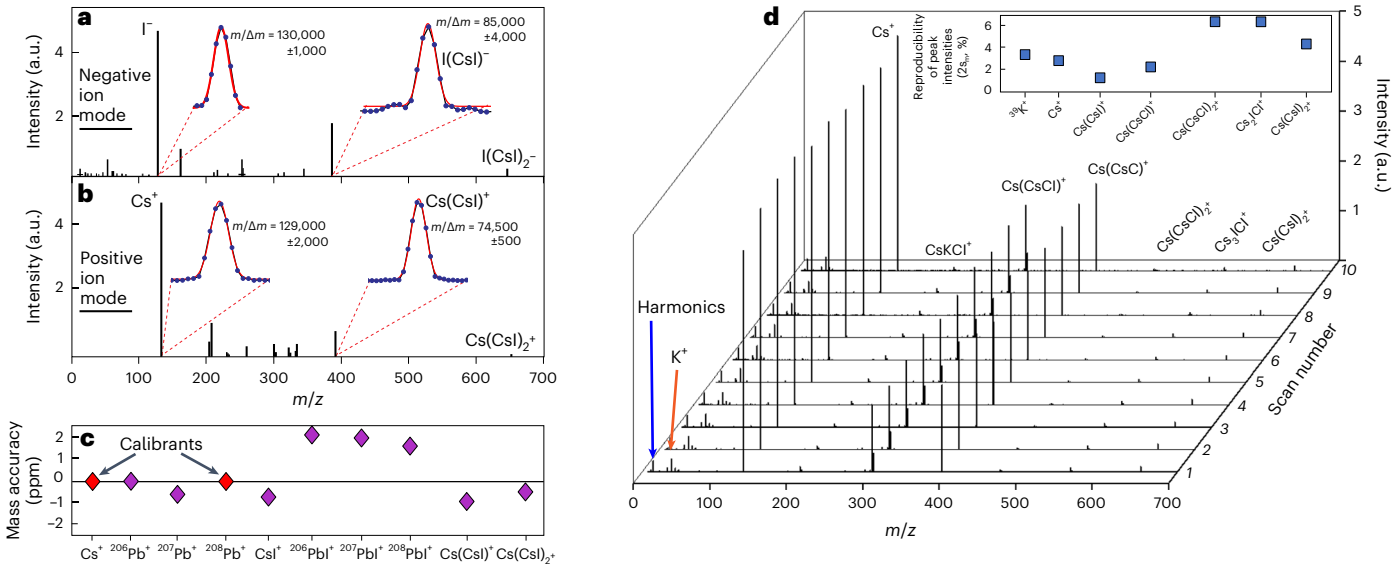

Fig. 2 | In both negative and positive mode, the miniaturized Orbitrap LDMS instrument achieves mass-resolving powers ($m/\Delta m$ > 10^5, FWHM at m/z 100) comparable to commercial standards. a,**b**, Spectra represent averages of 10 scans in the time domain collected in negative (**a**) and positive (**b**) mode, each acquired with an 800 ms transient (high resolution) and sampling rate of 5 MHz (Methods). Reported uncertainties of the mass-resolving powers of individual peaks are determined by the fit of a Gaussian curve (red curve) to the raw data (blue data points). **c**, Using $^{133}Cs^+$ as a single-point internal standard, and subsequently $^{133}Cs^+$ and $^{208}Pb^+$ (red diamonds) to apply a secondary linear calibration, analyte peaks (purple diamonds) fall within parts per million of exact monoisotopic masses. **d**, Single scans (10 total) collected in positive mode, acquired sequentially with 200 ms transients (medium resolution) and 5 MHz sampling rate, illustrate the reproducibility of the experiments. As shown in the inset, the peak intensities of $^{39}K^+$, Cs^+ and $Cs(CsI)^+$ all vary by less than 5% ($2s_m$) across all scans. Irradiance 0.1 GW cm^{-2}.

achieved by controlling the polarization of incident 532 nm light before conversion to 266 nm in the fourth harmonic; for comparison, the MOMA laser output energy can only be reduced to 10% of the maximum value by thermal detuning of the fourth harmonic crystal[22].

A longstanding issue for LDMS techniques has been the deduction of quantitative information, particularly relative and absolute abundances of elemental and molecular species. The reproducibility of LDMS peak intensities is limited by: (1) the heterogeneity of the sample, (2) shot-to-shot variability of the laser output energy and (3) dynamic changes in sample morphology induced by extended laser irradiation, which affect photon–substrate coupling. However, the empirical determination of relative sensitivity factors of elements with distinct electronic configurations, which have been shown to control laser-induced fractionation[23], can enable the quantification of concentration ratios[24] in solid samples. Absolute abundances can be further derived if an internal standard is known[25]. Such approaches, which are commonplace for laser ablation inductively coupled plasma mass spectrometry (LA-ICPMS), offer promise for the quantitation of spectral signals derived from LDMS analysis. However, substantial work remains to validate these models.

Measuring the relative abundances of organic molecules is even more challenging as observed signal intensities are sensitive to the absorption characteristics, bond strengths and ionization energy of the compound, as well as the physicochemical properties of the sample matrix and dynamics of the plasma plume. In spite of these challenges, linear responses between analyte concentrations and peak intensities normalized to an internal standard have enabled the quantitative analysis of amino acids[26], oligonucleotides[27] and a range of other organics[28] via LDMS techniques. Even without internal standardization, atomic and molecular ratios were captured with high reproducibility (better than ±10%, 2 standard error of the mean, $2s_m$) during the LDMS analysis of Cs under relatively constant operational conditions in this study (Supplementary Fig. 6).

Due to their identical electronic configurations and comparable physicochemical properties, isotopes of the same element (and isotopologues of the same molecule, to a lesser extent) are more easily preserved during an LDMS experiment. Isotopic precision is controlled largely by S/Ns, and thus the dynamic range of the sensor. The Orbitrap analyser, which can accommodate up to 10^6 elementary charges during a single analysis[29], has been shown to support a linear intrascan dynamic range up to 10^4 (ref. 30), providing access to low abundance isotopes down to 0.1 mol%. Although space-charge effects can incur isotope fractionation during transient acquisition[31], precise and accurate $^{13}C/^{12}C$ ratios measured for single species (for example, $^{13}C^{12}C_2H_8O_2N^+/^{12}C_3H_8O_2N^+$ in nominally pure alanine) within multicomponent sample mixtures have been recorded following careful calibration efforts, such as mass pre-filtering, transient length shortening, and/or external standardization with a matrix-matched reference material[32].

Results

A typical LDMS experiment comprises: (1) desorption/ionization of the sample via pulsed laser light, (2) acceleration, focusing and adjustment of the reference potential of analyte ions through the ion optics lens stack, (3) ion injection and electrodynamic squeezing in the trap and (4) detection of ion packets according to their respective axial frequencies, and hence m/z. Tunable laser energy (and by extension fluence, J cm^{-2}, and irradiance, W cm^{-2}) promotes the ionization of refractory organics and mineral phases via multiphoton absorption, supporting controlled fragmentation and disproportionation reactions to derive molecular structure by in-source decay[33]. The beam radius at the sample surface (r) is a customizable parameter within the limits of diffraction; with an effective focal length of 140 mm, nominal UV-beam diameter of 3.0 mm and beam quality factor $M^2 < 1.5$, the 266 nm laser system leveraged in this study could approach a diffraction limited radius of $r < 12$ µm. Such fine spatial resolution comes at the expense of total analyte throughput, which tracks with r^2 at a given fluence/irradiance. A microelectromechanical systems (MEMS) steering mirror inside the laser head, coupled with a set of deflector electrodes within the ion optics, allows the construction of two-dimensional chemical images

https://doi.org/10.1038/s41550-022-01866-x

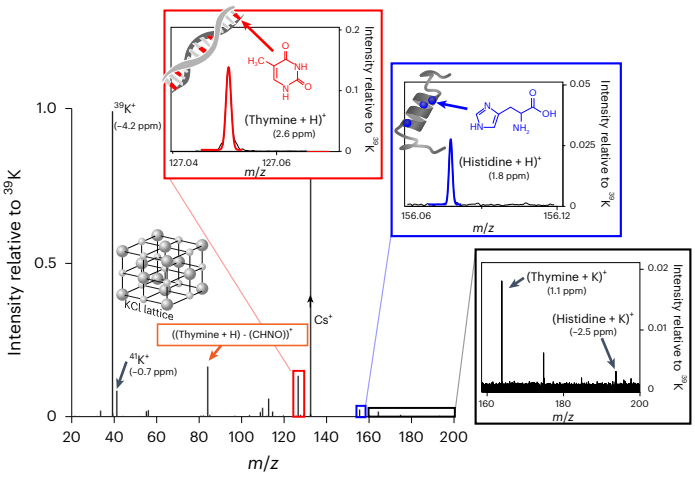

Fig. 3 | A single mass spectrum of an ocean world analogue sample illustrates the capability to detect and identify organic and inorganic components of planetary materials. The sample analysed was a residue of a salt-rich (0.32 wt% KCl) solution doped with trace levels of thymine and histidine, both biomarkers containing aromatic groups that effectively absorb UV radiation, without desalination of the sample. The area densities of thymine (180 pmol mm^{-2}) and histidine (210 pmol mm^{-2}) approximate those expected if 1 ml of ice derived from Enceladus' subsurface ocean was sublimated onto a cm^2 sample plate (main text). Detection of protonated molecular ions ([M + H]$^+$ shown with Gaussian fits for thymine (red) and histidine (blue)), diagnostic fragments ([M + H–CHNO]$^+$) and potassiated peaks (for example, [M + K]$^+$) provide corroborative identification of the analytes. The isotopic composition of K derived from the salt matrix falls within natural values. This spectrum represents a single scan acquired with an 800 ms transient and sampling rate of 5 MHz. $^{133}Cs^+$, sourced from the collocated CsI target, was used as an internal standard; $^{39}K^+$, $^{133}Cs^+$ and $^{208}Pb^+$ were used to apply a linear calibration. Irradiance 0.3 GW cm^{-2}.

with a nominal 500 µm diameter field of view (Supplementary Figs. 2 and 3) without requiring translation/rotation of the sample, facilitating the identification of biofabrics in situ.

The measurement of both positively and negatively charged particles provides complementary perspectives of complex chemical mixtures, empowering the detection of organic molecules with acidic and basic side chains as well as mineralogical indicators with high and low electronegativities. For example, positive and negative mass spectra of a finely ground CsI disc (Fig. 2), a common laboratory standard with identical composition to the calibrant for the MOMA flight instrument, provide multiple molecular fingerprints diagnostic of the substrate. In positive mode, CsI is exemplified by a high-intensity Cs^+ peak (m/z 132.9054), but also $Cs(CsI)^+$ (m/z 392.7153) and $Cs(CsI)_2^+$ (m/z 652.5253) clusters at lower signal intensities. In negative mode, the spectrum is dominated by I^- (m/z 126.9045) followed by $I(CsI)^-$ (m/z 386.7144) and $I(CsI)_2^-$ (m/z 646.5243). The mass resolution (for example, $m/\Delta m$ > 100,000, full-width at half-maximum (FWHM) at Cs^+) and parts per million level mass accuracy of these spectra, collected on the miniaturized prototype shown in Fig. 1, meet the performance specifications of commercial instruments; for example, the Thermo Scientific™ Q Exactive™ mass spectrometer offers mass resolution up to $m/\Delta m$ = 140,000 (FWHM) at m/z 200 with <3 ppm mass accuracy (r.m.s. with external calibration). Such analytical capabilities support the unambiguous identification of elemental and molecular signatures for both commercial and spaceflight applications.

Chloride salts, such as NaCl and KCl, are important planetary materials because they can depress the freezing point of liquid water in cryogenic environments and concentrate dilute monomers of more complex biomolecules (for example, RNA) via enhanced adsorption onto mineral surfaces[34]. Such salts have been observed on the surface of Europa[35], within the Enceladus plume[36], and inside Occator crater on the dwarf planet Ceres[37]. Consequently, to address high-priority astrobiology mission objectives[38–40], future payload investigations need to characterize salt-rich sample matrices to gain insights into the provenance of detected organics.

Assuming that the composition of Enceladus approximates that of a comet, as suggested by comparable volatile abundances and deuterium–hydrogen (D/H) ratios recorded in the plume[41] and those observed in cometary comae[42], measurements provided by the Cassini payload implicate up to parts per million by weight (ppmw) concentrations of individual amino acids in the subsurface ocean[43]. Area densities exceeding 200 pmol mm^{-2} are projected if 1 ml of water ice, the sample volume baselined for each instrument onboard the Europa Lander[38], was sublimated onto a cm^2 sample plate. The analysis of a salt-rich planetary analogue sample containing similar levels of a proteinogenic amino acid (that is, histidine) and nucleobase (that is, thymine) demonstrates the capacity of the Orbitrap LDMS instrument to simultaneously access both organic and inorganic fractions of multicomponent sample mixtures representative of those that may be collected by future missions to ocean worlds (Fig. 3).

The elucidation of molecular structure, including the differentiation of structural isomers, represents an orthogonal means to establish the identity of biomarkers and inform on the probability of biogenicity based on molecular complexity[2]. The finely controlled output energy of the laser source pioneered here enables in-source decay, a technique that has been shown to induce molecular fragmentation and facilitate the identification of peptides based on diagnostic amine-bond cleavages[44] and sequencing of proteins from the determination of N-terminal fragments[45] via matrix-assisted LDMS techniques. Another emerging capability specific to the Orbitrap analyser involves determining the distinct decay rate of each compound during time-resolved transient signal acquisition to calculate collision cross-section, a measure of ion size and conformation unique to each chemical species[46]. As a packet of ions of a specific m/z oscillates around the centre electrode, individual ions de-phase due primarily to elastic collisions with background gas, ion–ion interactions and other factors (for example, high-voltage ripple and field perturbations derived from mechanical imperfections)[47]. The additive effect of these processes results in degradative signal loss of ion packets as a function of time within the analyser.

As shown in Fig. 4, the decay profiles of select chemical species identified in Fig. 3 can be extracted from a single transient spectrum via FFT, followed by inverse FFT. The observed signal losses reflect the specific experimental conditions (for example, pressure, temperature and voltages) in addition to the additive decay factors described above. Chemical species that exhibit faster decay rates represent compounds with larger cross-sections, which reflect both m/z and molecular structure. Previous work has shown that the cross-sections of biogenic amino acids directly correlate with molecular weight, but aliphatic and aromatic compounds tend to be larger than the average trend due to inefficient folding[48]. Thus, collision cross-section determinations provide a complementary means to identify organic compounds and differentiate molecular structures, supporting agnostic detection techniques for the characterization of putative biomarkers.

The detection of organic compounds alone is insufficient to characterize the habitability potential of a cryogenic environment and/or assign prospects for extant or extinct life with high confidence. Exogenous infall can deliver considerable quantities of organic material to the surface of any planetary body; for reference, more than 10^7 kg of exogenous material is delivered to the Earth every year[49]. Although infall rates scale with planet mass and interplanetary dust fluxes vary as a function of heliocentric distance[50], measurable quantities of organic materials are continually being accumulated on Europa, Enceladus and other ocean worlds. Associations between detected organic compounds and host mineralogy, informed by major, minor and trace element abundances, are powerful tools for establishing the provenance of organic matter. Rare earth elements (REEs; that is, La

https://doi.org/10.1038/s41550-022-01866-x

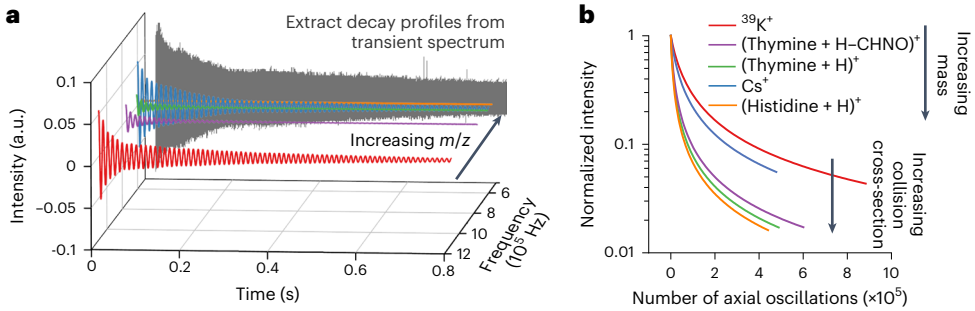

Fig. 4 | After successful injection into the Orbitrap analyser, the axial motions of the analyte ions are detected via image current in the time domain transient. a, The total transient signal (grey) may be decomposed into decay profiles of individual chemical species based on their distinctive frequencies (or *m*/*z*) via FFT and subsequent inverse FFT. The signal intensities of select peaks identified in Fig. 3 correlate with ion abundances (and to a lesser extent radial distribution about the centre electrode). **b**, The decay rates of signal intensities reflect ion losses as a function of time, informing on molecular weight and structure.

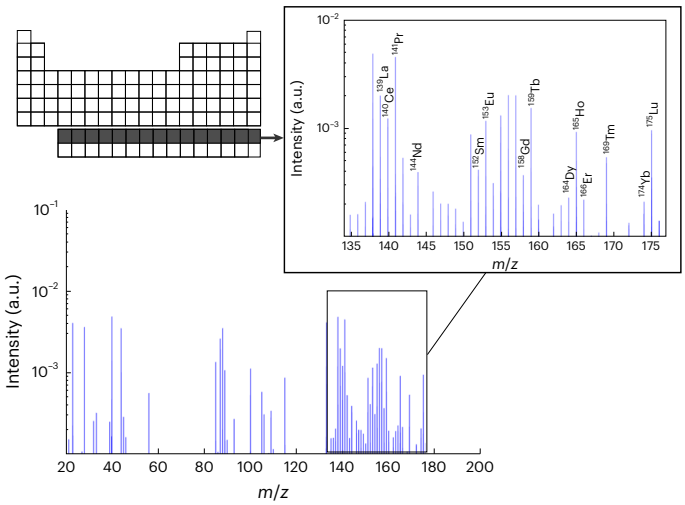

Fig. 5 | The Orbitrap LDMS instrument can detect trace elements down to ppmw concentrations, as illustrated by the measurement of REEs in NIST SRM610. Observed signal intensities reflect the distinct isotopic compositions and first ionization energies of each element. The detection limit for Pr, which is monoisotopic and has the lowest first ionization energy of the REEs, is 1.8 ppmw based on the observed S/N in this single spectrum. Summing multiple scans can reduce the noise floor and improve detection limits when time and energy resources are available. Irradiance 0.6 GW cm^{-2}.

through Lu) are particularly valuable proxies for geological sources as this suite of trace elements shares a common valence state (X^{3+}) and systematic contraction in ionic radii, resulting in predictable partitioning behaviours. Consequently, REEs are routinely used to understand the chemistry, formation and evolution of major terrestrial reservoirs[51]. The miniaturized LDMS described here can measure REEs down to ppmw levels in solid samples (Fig. 5), enabling insights into the sourcing of detected organic molecules, including biomarkers. However, a systematic evaluation is needed to constrain the accuracy of quantified elemental concentrations and the reproducibility of observed abundance patterns of organic molecules.

The capacity to catalogue the organic inventory of samples and simultaneously measure major, minor and trace elements (such as REEs) for geological/mineralogical context positions this instrument for a wide range of high-priority mission concepts, such as those focused on in situ life detection objectives at ocean worlds[38–40] and progressive exploration of both the lunar nearside and farside[52]. Near-term opportunities include the Enceladus Orbilander mission prioritized by the NASA (National Aeronautics and Space Administration) Planetary Science Decadal Survey[53] and robotic missions to the Moon supporting the NASA Artemis Program[54].

Methods

Sample preparation

A 2.2-mm-thick CsI finely ground disc (7.49 mm diameter) produced by Almaz Optics, Inc. was secured via interference fit inside a counter bore machined into the stainless steel sample plate and analysed daily to tune the voltages applied to the ion optical lenses (Supplementary Figs. 4 and 5), verify ion transmission and baseline performance and monitor for instrumental drift. To simulate a salt-rich ice sample from a potentially viable ocean world, a volume of deionized water (Milli-Q, 18.2 MΩ·cm resistivity at room temperature) was physically admixed with 0.32 wt% KCl (Sigma-Aldrich P9541; purity ≥99.0%), approaching the observed alkali salt content of Type III Enceladus plume ice particles collected by the Cassini CDA (Cosmic Dust Analyser[36]) and modelled salinity levels in Europa's ocean based on brine mobility in the ice crust[55]. The salt solution was doped with 190 ppmw thymine (Alfa Aesar A15879; 97%) and 280 ppmw L-histidine (Sigma-Aldrich P500108; 99.9%), both biomarkers offering high UV absorption (Supplementary Fig. 7). The organic-bearing sample was then agitated with a vortex mixer (2,800 rpm) to promote dissolution and homogenization. Before drop-casting, the sample plate was cleaned with isopropyl alcohol and acetone in sequence. Then 40 µl of the analogue solution were deposited onto the surface of the stainless steel sample plate over an area of 350 mm^2 and allowed to evaporate on a hot plate (115 °C) in a chemical fume hood; this desiccation step produced a heterogenous residue in line with what might be expected if an aliquot of ice was sublimated on a warm sample plate on a landed mission to Europa or Enceladus. The resultant sample residuum had an average area density of 180 pmol mm^{-2} thymine and 210 pmol mm^{-2} histidine. A disc of NIST SRM610 was installed into the stainless steel sample plate (alongside the CsI disc) to investigate the capacity of the miniaturized Orbitrap LDMS instrument to measure trace elements.

Measurement protocol

The Orbitrap analyser was located inside a Kimball Physics spherical cube vacuum chamber at pressure conditions found on the surface of Europa (that is, ≤10^{-6} Pa). A load lock chamber equipped with a dedicated pumping system and manual gate valve enabled isolation of the stainless steel plate during sample exchange, minimizing communication between the simulation chamber and laboratory atmosphere. After the sample was loaded onto the target plate, it was introduced to the Orbitrap chamber through the load lock via a linear-rotary actuator. The pressures in both chambers were monitored via hot-cathode ionization vacuum gauges; all analyses were conducted at pressures ≤4×10^{-6} Pa. Light emitted from the laser source (266 nm) passed

through a fused silica viewport window (>90% transmission at 266 nm) installed on the main vacuum chamber and irradiated the sample at an incident angle of 45°. The laser beam profile at the sample surface was measured at 80 × 120 µm, enabling fluences between 0.06 J cm^{-2} (at 1% max energy output) and 6 J cm^{-2} (at 100% max energy output) and irradiances between 0.01 GW cm^{-2} and 1 GW cm^{-2}. An external photodiode served to both detect each laser pulse and trigger subsequent operations (for example, voltage slewing) via a precise timing engine implemented in a field-programmable gate array (FPGA). Different sampling locations on the target plate were accessed by rotating the actuator.

Data processing

Each spectrum was collected at a sampling rate of 5 MHz for either 200 ms (medium resolution) or 800 ms (high resolution) transients. A custom LabVIEW-based software package[56] was used to regulate experimental sequences, including timing operations, voltage settings and ramp rates, data acquisition and data processing. Standard data processing techniques included applying Hanning apodization and zero-filling raw transient spectra before converting the signals to the frequency domain signal via FFT (Supplementary Fig. 8 and Supplementary Table 1). Each frequency spectrum was calibrated and translated into a conventional mass spectrum using a single peak (for example, $^{133}Cs^+$) as an internal standard, and two or more well-characterized peaks (for example, $^{133}Cs^+$ and $^{208}Pb^+$) to apply an additional linear term to the calibration. Mass accuracy was calculated as the deviation of the determined mass from the exact mass in parts per million. Mass-resolving powers, calculated at FWHM peak intensities, were determined using Gaussian peak-fitting functions. To determine collision cross-section, a peak of interest was isolated in the frequency domain and moved artificially to a lower frequency (reducing computing requirements); an inverse FFT enabled reconstruction of the decay profile of the selected ion packet. Chemical species with low S/Ns (for example, S/N < 10) were excluded from this practice because the high noise floor distorted peak shapes, resulting in inaccurate inversions of the decay profiles.

Data availability

Source data are provided with this paper. All other data presented in this study are available in the Supplementary Information.

References

1. Johnson, S. S., Anslyn, E. V., Graham, H. V., Mahaffy, P. R. & Ellington, A. D. Fingerprinting non-terran biosignatures. *Astrobiology* **18**, 915–922 (2018).
2. Marshall, S. M., Murray, A. R. G. & Cronin, L. A probabilistic framework for identifying biosignatures using Pathway Complexity. *Philos. Trans. R. Soc. Lond. A* **375**, 20160342 (2017).
3. Chan, M. A. et al. Deciphering biosignatures in planetary contexts. *Astrobiology* **19**, 1075–1102 (2019).
4. Neveu, M., Hays, L. E., Voytek, M. A., New, M. H. & Schulte, M. D. The ladder of life detection. *Astrobiology* **18**, 1375–1402 (2018).
5. Lukmanov, R. A. et al. On topological analysis of fs-LIMS data. Implications for in situ planetary mass spectrometry. *Front. Artif. Intell.* https://doi.org/10.3389/frai.2021.668163 (2021).
6. Johnston, S., Gehrels, G., Valencia, V. & Ruiz, J. Small-volume U–Pb zircon geochronology by laser ablation-multicollector-ICP-MS. *Chem. Geol.* **259**, 218–229 (2009).
7. Sagdeev, R. Z. & Zakharov, A. V. Brief history of the Phobos mission. *Nature* **341**, 581–585 (1989).
8. Managadze, G. G. et al. Study of the main geochemical characteristics of Phobos' regolith using laser time-of-flight mass spectrometry. *Sol. Syst. Res.* **44**, 376–384 (2010).
9. Goesmann, F. et al. The Mars Organic Molecule Analyzer (MOMA) instrument: characterization of organic material in Martian sediments. *Astrobiology* **17**, 655–685 (2017).
10. Grubisic, A. et al. Laser desorption mass spectrometry at Saturn's moon Titan. *Int. J. Mass Spectrom.* **470**, 116707 (2021).
11. Chumikov, A. E., Cheptsov, V. S., Managadze, N. G. & Managadze, G. G. LASMA-LR laser-ionization mass spectrometer onboard Luna-25 and Luna-27 missions. *Sol. Syst. Res.* **55**, 550–561 (2021).
12. Briois, C. et al. Orbitrap mass analyser for in situ characterisation of planetary environments: performance evaluation of a laboratory prototype. *Planet. Space Sci.* **131**, 33–45 (2016).
13. Willhite, L. et al. CORALS: a laser desorption/ablation Orbitrap mass spectrometer for in situ exploration of Europa. In *2021 IEEE Aerospace Conference* **50100**, 1–13 (2021).
14. Makarov, A. A. Mass spectrometer US patent 5,886,346 (1999).
15. Arevalo, R. Jr, Ni, Z. & Danell, R. M. Mass spectrometry and planetary exploration: a brief review and future projection. *J. Mass Spectrom.* **55**, e4454 (2020).
16. Makarov, A. Electrostatic axially harmonic orbital trapping: a high-performance technique of mass analysis. *Anal. Chem.* **72**, 1156–1162 (2000).
17. Arevalo, R. Jr et al. An Orbitrap-based laser desorption/ablation mass spectrometer designed for spaceflight. *Rapid Commun. Mass Spectrom.* https://doi.org/10.1002/rcm.8244 (2018).
18. Yu, A. W. et al. The Lunar Orbiter Laser Altimeter (LOLA) laser transmitter. In *2011 IEEE International Geoscience and Remote Sensing Symposium* 3378–3379 (2011).
19. Malloci, G., Mulas, G. & Joblin, C. Electronic absorption spectra of PAHs up to vacuum UV. *Astron. Astrophys.* **426**, 105–117 (2004).
20. Cloutis, E. A. et al. Ultraviolet spectral reflectance properties of common planetary minerals. *Icarus* **197**, 321–347 (2008).
21. Fahey, M. et al. Ultraviolet laser development for planetary lander missions. In *2020 IEEE Aerospace Conference* 1–11 (2020).
22. Büttner, A. et al. Optical design and characterization of the MOMA laser head flight model for the ExoMars 2020 mission. In *Proc. SPIE 11180, International Conference on Space Optics—ICSO* **2018**, 111805H (12 July 2019); https://doi.org/10.1117/12.2536116
23. Jenner, F. E. & O'Neill, H. S. C. Major and trace analysis of basaltic glasses by laser-ablation ICP-MS. *Geochem. Geophys. Geosyst.* https://doi.org/10.1029/2011GC003890 (2012).
24. Humayun, M., Davis, F. A. & Hirschmann, M. M. Major element analysis of natural silicates by laser ablation ICP-MS. *J. Anal. Spectrom.* **25**, 998–1005 (2010).
25. Longerich, H. P., Günther, D. & Jackson, S. E. Elemental fractionation in laser ablation inductively coupled plasma mass spectrometry. *Fresenius J. Anal. Chem.* **355**, 538–542 (1996).
26. Alterman, M. A., Gogichayeva, N. V. & Kornilayev, B. A. Matrix-assisted laser desorption/ionization time-of-flight mass spectrometry-based amino acid analysis. *Anal. Biochem.* **335**, 184–191 (2004).
27. Sarracino, D. & Richert, C. Quantitative MALDI-TOF MS of oligonucleotides and a nuclease assay. *Bioorg. Med. Chem. Lett.* **6**, 2543–2548 (1996).
28. Chumbley, C. W. et al. Absolute quantitative MALDI imaging mass spectrometry: a case of rifampicin in liver tissues. *Anal. Chem.* **88**, 2392–2398 (2016).
29. Zubarev, R. A. & Makarov, A. Orbitrap mass spectrometry. *Anal. Chem.* **85**, 5288–5296 (2013).
30. Makarov, A., Denisov, E., Lange, O. & Horning, S. Dynamic range of mass accuracy in LTQ Orbitrap hybrid mass spectrometer. *J. Am. Soc. Mass Spectrom.* **17**, 977–982 (2006).
31. Hoegg, E. D. et al. Isotope ratio characteristics and sensitivity for uranium determinations using a liquid sampling–atmospheric pressure glow discharge ion source coupled to an Orbitrap mass analyzer. *J. Anal. Spectrom.* **31**, 2355–2362 (2016).

32. Hofmann, A. E. et al. Using Orbitrap mass spectrometry to assess the isotopic compositions of individual compounds in mixtures. *Int. J. Mass Spectrom.* **457**, 116410 (2020).
33. Hardouin, J. Protein sequence information by matrix-assisted laser desorption/ionization in-source decay mass spectrometry. *Mass Spectrom. Rev.* **26**, 672–682 (2007).
34. Franchi, M., Ferris, J. P. & Gallori, E. Cations as mediators of the adsorption of nucleic acids on clay surfaces in prebiotic environments. *Orig. Life Evol. Biosph.* **33**, 1–16 (2003); https://doi.org/10.1023/A:1023982008714
35. Trumbo, S. K., Brown, M. E. & Hand, K. P. Sodium chloride on the surface of Europa. *Sci. Adv.* **5**, eaaw7123 (2019).
36. Postberg, F., Schmidt, J., Hillier, J. et al. A salt-water reservoir as the source of a compositionally stratified plume on Enceladus. *Nature* **474**, 620–622 (2011).
37. De Sanctis, M. C. et al. Fresh emplacement of hydrated sodium chloride on Ceres from ascending salty fluids. *Nat. Astron.* **4**, 786–793 (2020).
38. Hand, K. P. et al. *Report of the Europa Lander Science Definition Team* (NASA, 2017).
39. Hendrix, A. R. et al. The NASA Roadmap to Ocean Worlds. *Astrobiology* **19**, 1–27 (2018); https://doi.org/10.1089/ast.2018.1955
40. MacKenzie, S. M. et al. The Enceladus Orbilander mission concept: balancing return and resources in the search for life. *Planet. Sci. J.* **2**, 77 (2021).
41. Waite, J. H. Jr et al. Liquid water on Enceladus from observations of ammonia and ^{40}Ar in the plume. *Nature* **460**, 487–490 (2009).
42. Altwegg, K., Balsiger, H. & Fuselier, S. A. Cometary chemistry and the origin of icy solar system bodies: the view after Rosetta. *Annu. Rev. Astron. Astrophys.* **57**, 113–155 (2019).
43. Guzman, M. et al. Collecting amino acids in the Enceladus plume. *Int. J. Astrobiol.* **18**, 47–59 (2018).
44. Takayama, M. In-source decay characteristics of peptides in matrix-assisted laser desorption/ionization time-of-flight mass spectrometry. *J. Am. Soc. Mass Spectrom.* **12**, 420–427 (2001).
45. Katta, V., Chow, D. T. & Rohde, M. F. Applications of in-source fragmentation of protein ions for direct sequence analysis by delayed extraction MALDI-TOF mass spectrometry. *Anal. Chem.* **70**, 4410–4416 (1998).
46. Sanders, J. D. et al. Determination of collision cross-sections of protein ions in an Orbitrap mass analyzer. *Anal. Chem.* **90**, 5896–5902 (2018).
47. Makarov, A. & Denisov, E. Dynamics of ions of intact proteins in the Orbitrap mass analyzer. *J. Am. Soc. Mass Spectrom.* **20**, 1486–1495 (2009).
48. Anupriya, Jones, C. A. & Dearden, D. V. Collision cross sections for 20 protonated amino acids: Fourier transform ion cyclotron resonance and ion mobility results. *J. Am. Soc. Mass Spectrom.* **27**, 1366–1375 (2016).
49. Chyba, C. & Sagan, C. Endogenous production, exogenous delivery and impact-shock synthesis of organic molecules: an inventory for the origins of life. *Nature* **355**, 125–132 (1992).
50. Poppe, A. R. An improved model for interplanetary dust fluxes in the outer Solar System. *Icarus* **264**, 369–386 (2016).
51. Taylor, S. R. & McLennan, S. M. in *Handbook on the Physics and Chemistry of Rare Earths* Vol. **11**, 485–578 (eds Gschneidner, K. A. J. & Eyring, l.) (Elsevier, 1988).
52. Jawin, E. R. et al. Lunar science for landed missions workshop findings report. *Earth Space Sci.* **6**, 2–40 (2019).
53. National Academies of Sciences, Engineering, and Medicine. *Origins, Worlds, and Life: A Decadal Strategy for Planetary Science and Astrobiology 2023–2032* (National Academies Press, 2022).
54. *Artemis III Science Definition Team Report* (NASA, 2020).
55. Steinbrügge, G. et al. Brine migration and impact-induced cryovolcanism on Europa. *Geophys. Res. Lett.* **47**, e2020GL090797 (2020).
56. Danell, R. et al. A full featured, flexible, and inexpensive 2D and 3D ion trap control architecture and software package. In *Proc. 58th ASMS Conference on Mass Spectrometry and Allied Topics* 283889 (2010).

Acknowledgements

This study was supported by the University of Maryland Faculty Incentive Program (PI: R.A. Jr), NASA Goddard Space Flight Center Internal Research and Development Program (PIs: A.G. and A.Y.), NASA ROSES ICEE 2 Grant 80NSSC19K0610 (PI: R.A. Jr), ROSES DALI Grant 80NSSC19K0768 (PI: R.A. Jr) and CRESST II Award Number 80GSFC21M0002 (PI: A.S.).

Author contributions

The dataset presented in this study was collected and analysed by R.A. Jr, L.W., A.B., Z.N. and S.R. The system-level architecture of the miniaturized instrument and the operational sequence of the experiments conducted were defined by R.A. Jr, A.S., R.D., A.G., C.B., L.T., F.C. and A.M. Requirements for the ion optics and SIMION models of ion transmission were provided by A.S. The mechanical design of the mass analyser assembly and custom series of ion optics were led by C.G. and N.M. The design and build of the prototype UV laser system was led by A.Y. and M.F. All authors contributed to the interpretation of the results and editing of the manuscript.

Competing interests

A.M. is an employee of Thermo Fisher Scientific, the manufacturer of the Orbitrap device leveraged in the miniaturized instrument described here.

Additional information

Supplementary information The online version contains supplementary material available at https://doi.org/10.1038/s41550-022-01866-x.

Correspondence and requests for materials should be addressed to Ricardo Arevalo.

Peer review information *Nature Astronomy* thanks Marek Tulej and the other, anonymous, reviewer(s) for their contribution to the peer review of this work.